Journal of Electronic Imaging

JElectronicImaging.org

Automatic detection method for mura defects on display film surface using modified Weber's law

Myung-Muk Kim
Seung-Ho Lee

Automatic detection method for mura defects on display film surface using modified Weber's law

Myung-Muk Kim[a] and Seung-Ho Lee[b,*]
[a]Korea Aerospace Research Institute, Satellite Information Research Laboratory, Satellite Operations Division, Low Earth Orbit Satellite Mission Operation Team, 169-84, Gwahangno, Yuseong-gu, Daejeon 305-719, Republic of Korea
[b]Hanbat National University, Department of Electronics & Control Engineering , 125, Dongseo-daero, Yuseong-gu, Daejeon 305-719, Republic of Korea

Abstract. We propose a method that automatically detects mura defects on display film surfaces using a modified version of Weber's law. The proposed method detects mura defects regardless of their properties and shapes by identifying regions perceived by human vision as mura using the brightness of pixel and image distribution ratio of mura in an image histogram. The proposed detection method comprises five stages. In the first stage, the display film surface image is acquired and a gray-level shift performed. In the second and third stages, the image histogram is acquired and analyzed, respectively. In the fourth stage, the mura range is acquired. This is followed by postprocessing in the fifth stage. Evaluations of the proposed method conducted using 200 display film mura image samples indicate a maximum detection rate of ~95.5%. Further, the results of application of the Semu index for luminance mura in flat panel display (FPD) image quality inspection indicate that the proposed method is more reliable than a popular conventional method. *© 2014 SPIE and IS&T* [DOI: 10.1117/1.JEI.23.4.043019]

Keywords: Weber's law; mura; image histogram; Semu index; FPD; pixel ratio.

Paper 14042 received Feb. 10, 2014; revised manuscript received Jun. 11, 2014; accepted for publication Jul. 2, 2014; published online Aug. 6, 2014.

1 Introduction

Concomitant with the expansion of the display market, especially due to devices such as smartphones and large LCD TVs, the display industry has rapidly advanced in recent years, with businesses in the display market vying to achieve higher yields than their competitors. The most influential factor in determining yield rate is mura defects on the display film surface. The mura phenomenon refers to the local lightness variation with partially or entirely nonuniform chrominance in display films. Methods for detecting such muras on the display film surface broadly include detections in the spatial and frequency domains. In particular, methods for early detection of scratch and blob mura in those domains have been proposed.[1,2] Because of the varied types of muras that exist, it is difficult to derive an accurate mathematical model for muras. As a result, prior to the introduction of a fuzzy neural network,[3] a combination of fuzzy logic and neural network, only one type of mura was detected. Prior to the recent proposal of methods such as hough transform (HT) (Ref. 4) and discrete cosine transform (DCT),[5] mura was conventionally detected in the frequency domain via wavelet transform. However, the characteristics of mura images make handling several types of mura images very difficult, and hence, evidence for detectability factor and accuracy of patterns is lacking. In this paper, our goal is to detect mura and validate the accuracy of the results obtained for different mura types by detecting the regions perceived by human vision.

Haun and Peli[6] conducted human visual perception studies in which they analyzed the experimental results of two images with the same phase spectrum randomly assigned to attain spectrum amplitude and compared the external contrast. Their test results indicated that contrast is identified in between uniform contrast values and stiles[7] as illustrated with a threshold value or the smallest perceptible quantity for the convenience of the color matching process. Further, Van Nes and Bouman[8] deduced contrast sensitivity functions in the frequency domain from the diffraction caused by light scattering within the retina and nerve transmission system. Whittle[9] suggested that the threshold to differentiate luminance can be classified in proportion to the absolute luminance up to the black limit. A specific threshold value is necessary to recognize such stimulations in human vision. Thus, in this paper, muras on the display film surface are detected based on Weber's constant for human vision and a histogram that illustrates image information. Figure 1 shows muras on a display film surface, while Fig. 2 shows images of display film mura, such as scratches, dust, and impurities, introduced during the display manufacturing process.

This paper proposes an automatic mura detection method that uses a modified version of Weber's law that uses the relative stimulus intensity as a standard. We determine our proposed method's display film mura defects detection rate using 200 sample images with mura and verify its reliability via the Semu index[10] for luminance mura in FPD image quality inspection according to the SEMI standard.

2 Research Trends

Mura detection is one of the most popular research areas among automatic detection methods using machine vision. Mura detection methods are classified into two types:

*Address all correspondence to: Seung-Ho Lee, E-mail: shlee@cad.hanbat.ac.kr

Fig. 1 Muras on display film surface.

detection in the spatial domain and detection in the frequency domain.

Tzu and Chou[11] proposed an automatic optical detection method for detecting spot muras in the spatial domain. They reported a substantial improvement in detecting spot mura using the tendency that black mura and white mura are visible through the commission international de l'eclairage (CIE) profile. However, their study was deficient because there was no objective estimation of other muras except for spot mura and detection rate.

Oh et al.[2] proposed a frequency-domain method that detects blob mura in thin film transistor (TFT)-LCD using wavelet transforms. Their method detects mura by eliminating unnecessary elements in the first- and second-generation wavelet transforms. The proposed method finds all blob muras in a panel; however, its detection area is limited. Further, the method detects only blob mura among various forms of mura. Chen and Kuo[5] presented a method that detects mura by reconstructing the background image after determining the cut-off frequency from the DCT coefficient of the mura image. Their method effectively detects various sizes, shapes, and categories of mura. However, it has difficulty in detecting muras that have a small difference in contrast with the background. Lee et al.[12] proposed a method that detects the background using an original clean panel image without any mura defects and accelerated wavelet multiresolution. Detecting mura defects using the original clean panel image is effective; however, if no original clean panel image exists, detection is difficult. Further, if the position of images taken by a camera does not accurately match the original clean panel image, accurate mura detection is also difficult.

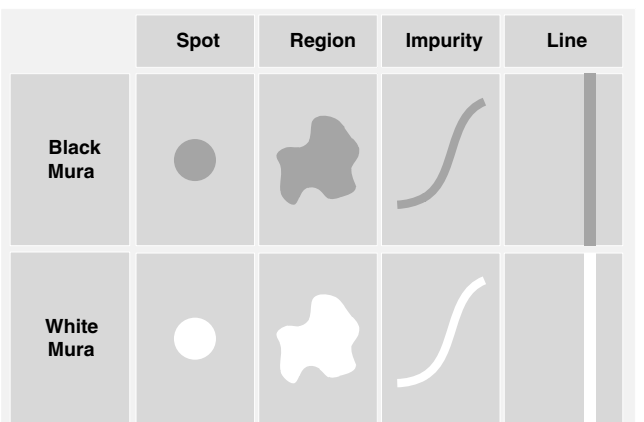

Fig. 2 Types of mura.

Jong et al.[13] proposed a method that selectively detects mura by simulating human vision among all the muras detected after removing the high-frequency elements in low-contrast images. However, they fell short of objective evaluations as their detection results did not include various forms of mura. Li and Tsai[4] proposed a method that detects mura based on the linear shape and pixel distance of the profile produced by improved Hough transform. The method shows high detection rates for muras of various shapes and has a high detection rate accuracy as verified by Semu. However, depending on the images, the limitation ranges of parameters in the Hough transform had to be determined differently, and many processes were needed, e.g., conducting the Hough transform in perpendicular and horizontal directions with wavelet transform. Zhuang and Ding[14] proposed a method that detects mura by detecting the mura edge using part of the results of a segmentation process based on the level set, after eliminating the background using a Gabor filter. Semu evaluation proves that the method has a high detection rate; however, it has difficulties, such as parameter changes, depending on image contrast for detection.

Other proposed mura detection methods include a method that combines the advantages of fuzzy logic and neural network to derive an accurate mathematical model[3] and a method that determines the cause of mura in photomask.[15] In the early stages, the trend in mura detection research was to detect a specific shape of mura in each area. The algorithms were subsequently modified, improved, and merged to detect all of the various shapes of mura. In addition, human vision as a standard started to be considered for detection results evaluation using Semu. However, previous research utilized complicated algorithms and the image samples used for evaluation did not have various mura.

In our study, we focus on detecting mura using a simple algorithm and the characteristics of vision in Weber's law for various image samples. The detection rates of research studies based on Weber's law are higher than that of other research studies.[16] The procedure used by our algorithm is as follows. In the first stage, mura images are obtained via a machine vision image acquisition procedure. In the second stage, a histogram of the acquired image is obtained. In the third stage, the histogram is analyzed by applying Weber's law. In the fourth and fifth stages, the position of the mura is recognized in the analyzed histogram and the final mura is detected using a median filter. The proposed method detects the area by simulating human vision, and muras are detectable regardless of their shape.

The remainder of this paper is organized as follows. Section 3 introduces Weber's law, the histogram, and our proposed method. Section 4 describes the validation process of our proposed method for mura detection rate and reliability evaluation using Semu. Finally, Sec. 5 summarizes and outlines our plans for future research.

3 Proposed Method

The automatic display film mura detection method proposed in this paper using a modified version of Weber's law comprises the five stages shown in Fig. 3. In the first stage, image

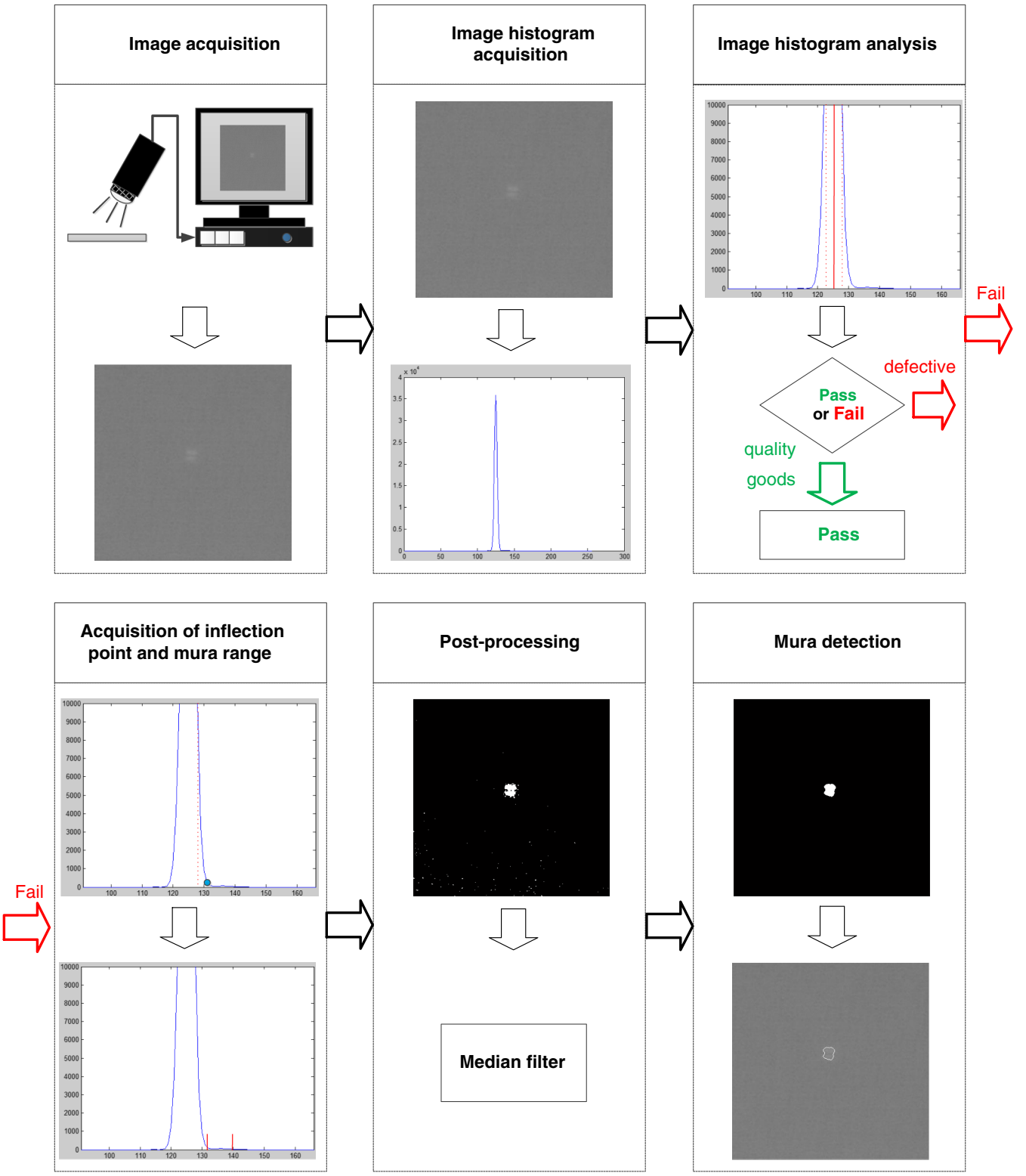

Fig. 3 Block diagram of the proposed method.

acquisition and gray-level shifting is carried out. This is followed in the second stage by acquisition of the image histogram. In the third stage, the mura presence is determined via histogram analysis. In the fourth stage, the inflection point and mura range are acquired. Finally, in the fifth stage, the mura is detected.

3.1 *Weber's Law*

Weber's law was first introduced by the German physiologist Ernst Heinrich Weber. It is a psychological law that states that the magnitude of the noticeable difference between two stimuli is proportional to the original stimulus value. Further, it is the minimum amount by which stimulus intensity must

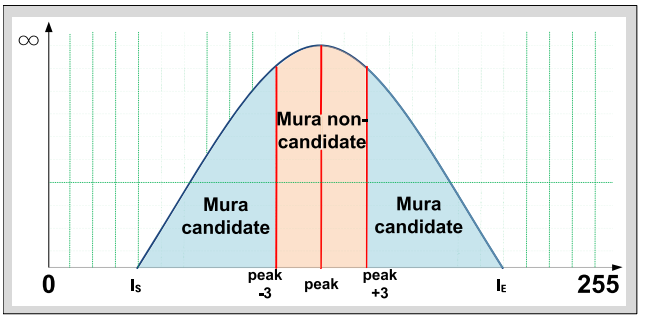

Fig. 4 Classification of candidate and noncandidate mura in image histogram.

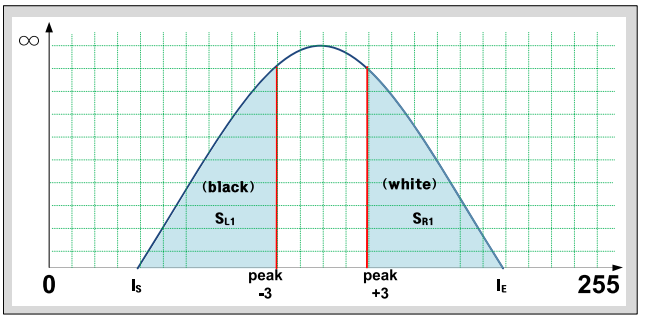

Fig. 5 Determination of mura direction.

be changed in order to produce a noticeable variation in sensory experience. The relative stimulus increments indirectly or directly perceived in daily living are as follows. In a noisy environment, one has to shout to be heard, whereas a whisper suffices in a quiet room. In a similar fashion, light-emitting devices, such as fluorescent lamps and flashlights, are brighter during the night than in the day. The law can be defined as

$$K = \frac{(R_2 - R_1)}{R_1} = \frac{\Delta R}{R_1}, \tag{1}$$

where K is a constant called the Weber fraction, R_1 is the initial stimulus intensity, R_2 is the second stimulus intensity, and ΔR is the differential threshold.

The method proposed in this paper detects mura defects that are unpleasant to human vision by defining the relative difference in the shapes, components, and other features of mura with various characteristics. The two main phases of the mura detection method that incorporate Weber's law are image histogram analysis and acquisition of inflection point and mura region.

3.2 *Image Histogram Acquisition*

The algorithm proposed in this paper does not apply Weber's law to the spatial-domain image, but instead applies it in the

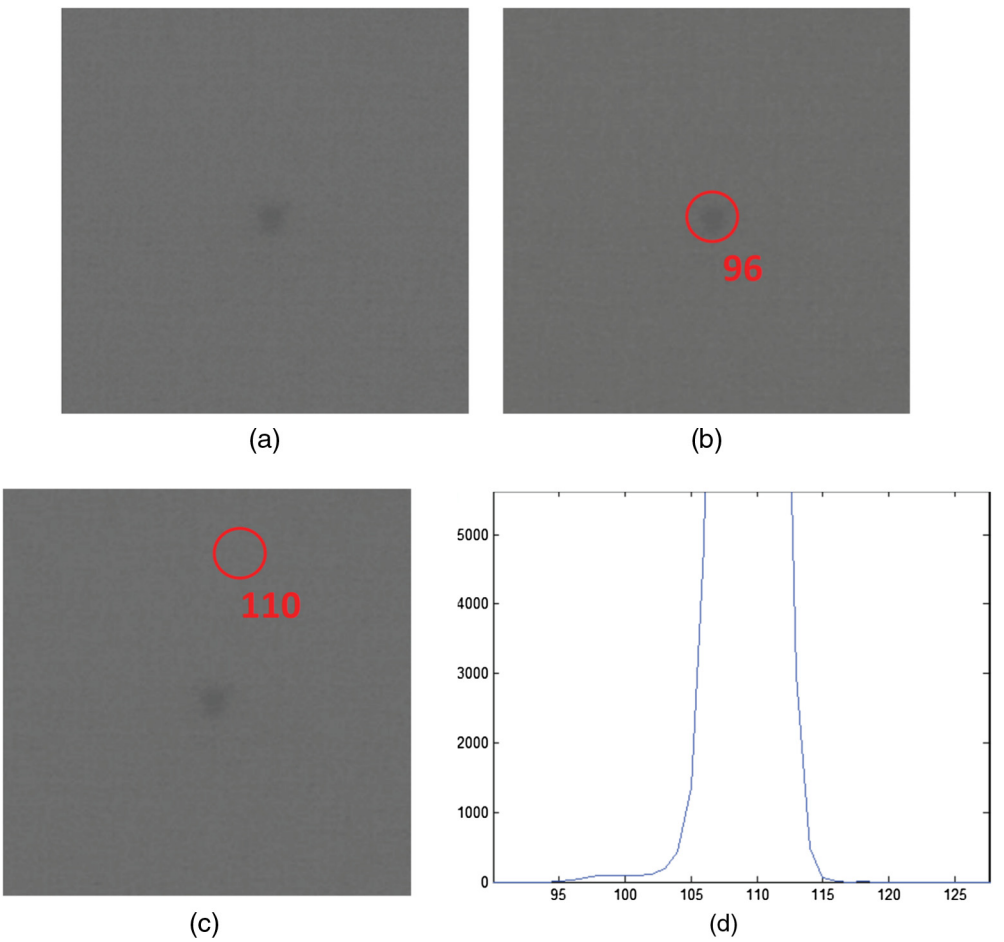

Fig. 6 Characteristics of image with black mura: (a) original image, (b) mura pixel value, (c) background pixel value, and (d) image histogram of (a).

acquisition of an image histogram with pixel information from an image. The image histogram is composed as follows:

$$h(r_k) = n_k, \tag{2}$$

where $h(r_k)$ is the histogram of the image, r_k is the k'th intensity level in the interval [0, G], n_k is the number of pixels in the image whose intensity level is rk, and G is the gray-level ranging from 0 to 255.

3.3 *Image Histogram Analysis*

Our proposed method does not use the absolute stimulus intensity defined by the characteristics of mura shapes, but instead finds muras using a relative stimulus difference from pixel number variations perceived by the sensory system. For this reason, determining the presence of black and white mura is crucial. Therefore, the image has to be divided into background, which is the major component of the image histogram, and mura defects, which are minor components of the image histogram.

In Fig. 4, the peak is the intensity at the highest point in the image histogram, where I_s and I_e are the starting and endpoint of the image histogram, respectively. The brightest pixels in the image are in the peak and background, the main component. On the other hand, mura defects have different pixel values compared to the background and fewer bright pixels to compare to the peak. The presence of mura is determined under a supposition that an image has pixel intensity values ranging from 0 to 255 by applying the visual constant, 1/100 of Weber's law:

$$G_K = \frac{256}{100} = 2.56 \approx 3, \tag{3}$$

where G_K denotes the Weber fraction of the gray-level range.

In Fig. 5, the range between the peak ± 3 is determined as the non-mura regions because visual recognition of mura defects is difficult. The remaining ranges are designated as mura candidates. The associated equation is as follows:

$$\begin{cases} \text{Peak} - 3 \le \text{Peak}, \text{Peak} + 3 \ge \text{Peak} & = \text{mura noncandidate} \\ \text{other} & = \text{mura candidate} \end{cases}. \tag{4}$$

The pixel values closer to zero on the left side are black mura, whereas those closer to 255 on the right side are white mura in the image histogram. The location of mura is

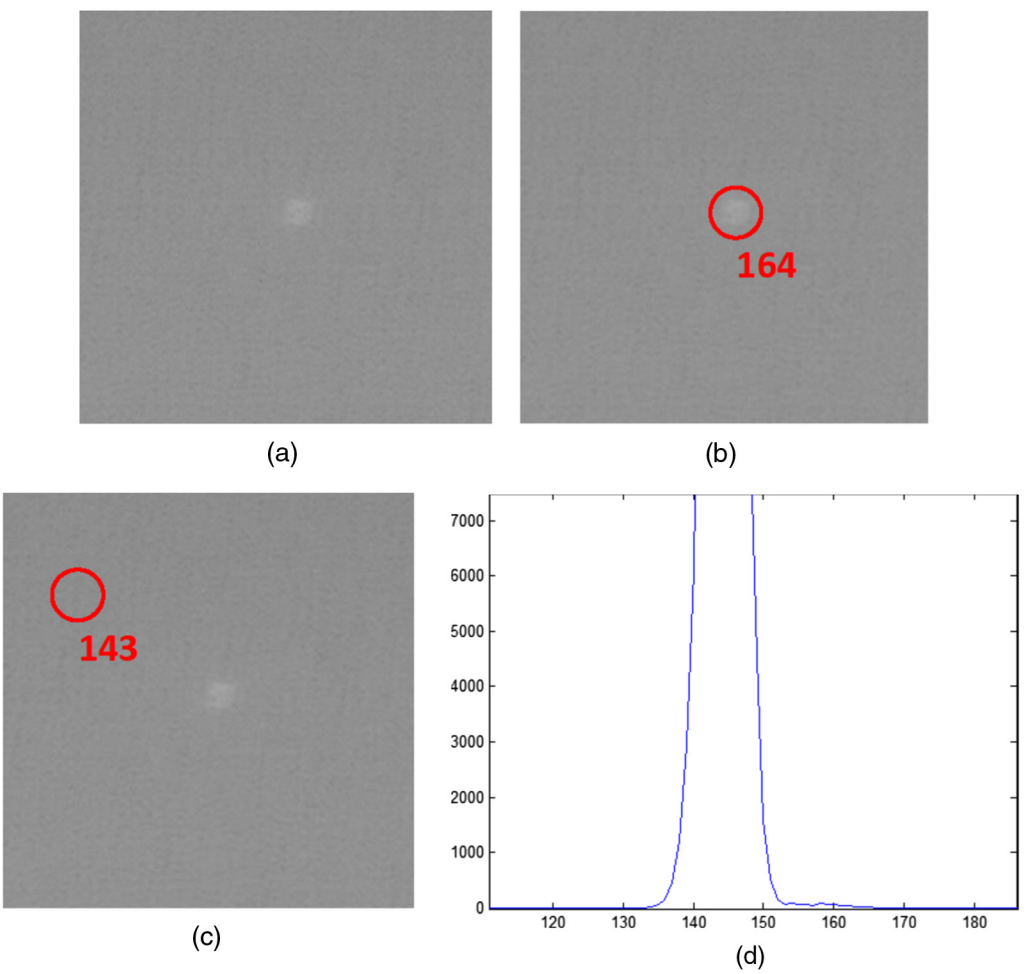

Fig. 7 Characteristics of image with white mura: (a) original image, (b) mura pixel value, (c) background pixel value, and (d) image histogram of (a).

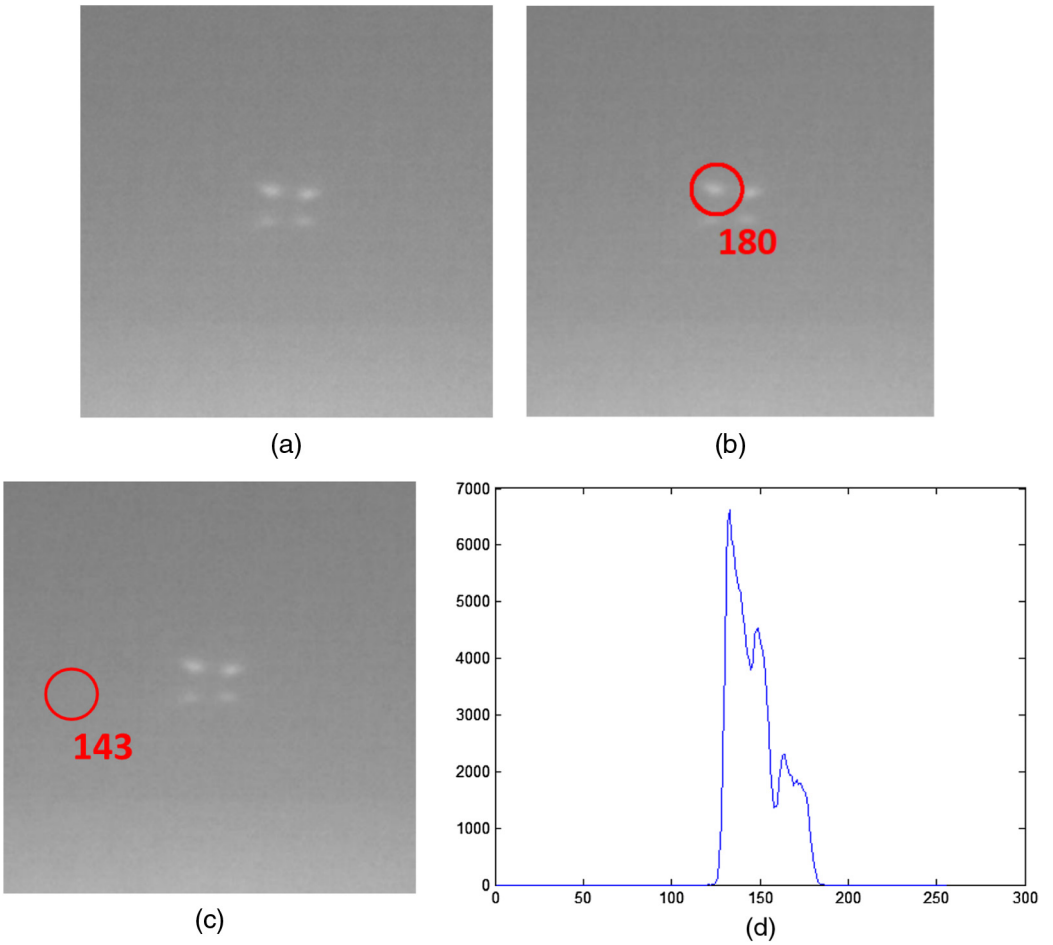

Fig. 8 Characteristics of corrupted image: (a) original image, (b) mura pixel value, (c) background pixel value, and (d) image histogram of (a).

determined on the basis of comparison between the sums of black and white pixels.

Figure 6 shows the characteristics of an image with black mura. The mura pixel value is ~96 in Fig. 6(b), and the background pixel value is ~110 in Fig. 6(c). In the image with the black mura, the mura is located on the left side of the image histogram, as shown in Fig. 6(d). Figure 7 illustrates the characteristics of an image with white mura. The mura pixel value is ~164 in Fig. 7(b), and the background pixel value is ~143 in Fig. 7(c). In the image with the white mura, the mura is located on the right side of the image histogram, as shown in Fig. 7(d). The mura direction in Figs. 6 and 7 can be obtained using Eq. (5). However, Eq. (5) may give the wrong direction when it is applied to an image histogram that is corrupted as a result of illumination components, such as the image shown in Fig. 8(d). To prevent this kind of error, mura direction is determined using Eq. (6), instead of Eq. (5), when the range of the image histogram exceeds 65 by ~40%.

Table 1 Mura range according to image ratio.

Ratio (rate)	Range (V)
<1.35	4
1.35 to 1.8	5
1.8 to 2.3	6
2.3 to 4.3	7
4.3 to 23	8
23 to 105	9
>105	~10
Otherwise	0

$$S_L = \sum_{A=I_S}^{\text{Peak}-3} x(A), \quad S_R = \sum_{B=\text{Peak}+3}^{I_E} x(B), \tag{5}$$

$$S_L = \sum_{C=I_S}^{I_S+7} x(C), \quad S_R = \sum_{D=I_E-7}^{I_E} x(D), \tag{6}$$

$$\begin{cases} I_E - I_S \geq 65 \text{ then } S_L = \sum_{C=I_S}^{I_S+7} x(C), & S_R = \sum_{D=I_E-7}^{I_E} x(D) \\ \text{other} & S_L = \sum_{A=I_S}^{Peak-3} x(A), \; S_R = \sum_{B=\text{Peak}+3}^{I_E} x(B) \end{cases}, \tag{7}$$

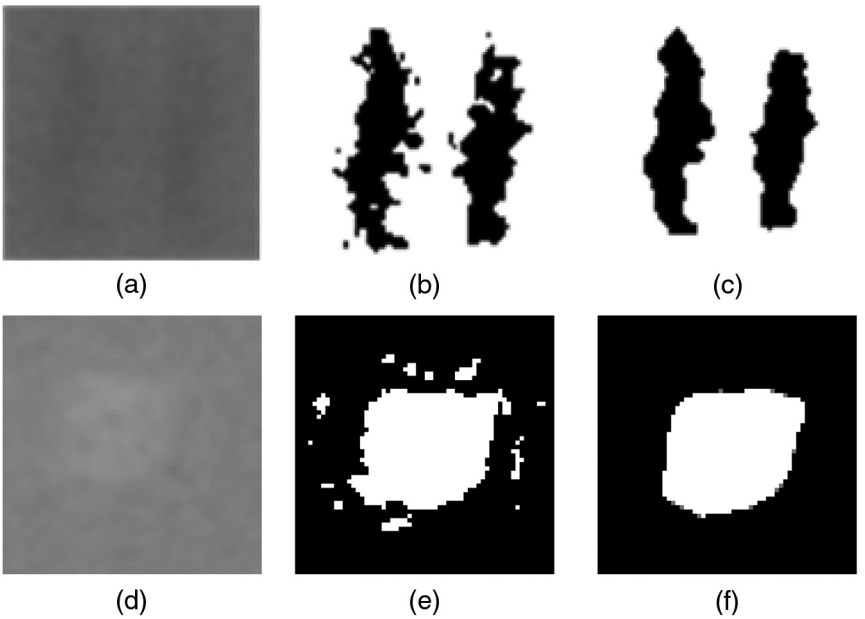

Fig. 9 Median filtering: (a) black mura original image, (b) mura range detection image of (a), (c) median filter applied to image of (b), (d) light mura original image, (e) mura range detection image of (d), and (f) median filter applied to image of (e).

$$\begin{cases} S_L & \text{then dark mura} \\ S_L > S_R & \text{then white mura} \end{cases}, \tag{8}$$

where S_L is the sum of all pixel values in the black area, the left side of the image histogram, and S_R is the sum of all pixel values in the white area, the right side of the image histogram.

3.4 *Acquisition of Inflection Point and Mura Range*

When the mura direction is determined, the position of the inflection point, the border point between the mura and the background, is obtained in the area with the mura direction as follows:

$$P_G = \text{Max}(|H''(I_S)|) \quad (0 \le I_S < \text{Peak} - 3), \tag{9}$$

where P_G is the inflection point and is applied to the image with the white mura by reversing it. Mura detection is done by designating the mura region from the obtained inflection point. The mura region is designated with the ratio from left to right pixel values in the image histogram. The equations for the ratio of the image are as follows:

$$\text{Cen} = \frac{I_S + I_E}{2}, \tag{10}$$

$$L = \sum_{E=I_S}^{\text{Cen}} x(E), \quad R = \sum_{F=\text{Cen}}^{I_E} x(F), \tag{11}$$

$$\begin{cases} (R - L) \ge 0 & R_{t1} = R_1, \quad R_{t2} = R_2 \\ \text{else} & R_{t1} = R_2, \quad R_{t2} = R_1 \end{cases} \tag{12}$$

$$\text{Rate} = \frac{R_{t1} - R_{t2}}{R_{t2}} \times 2.2, \tag{13}$$

where Cen is the center of the image histogram, L is the sum of the pixels on the left side of the image histogram, R is the sum of the pixels on the right side of the image histogram, and Rate is the image ratio. In Eq. (13), 2.2 is a constant value for expressing Rate. The image ratio closest to one is located at the same center and peak pixel, implying stable distributions of R and L. This can be determined on the basis of mura defects that are visually indistinguishable from the background image or have soft changes. This kind of mura that has considerable sensitivity has a small range. On the other hand, image ratios far from one are located at different pixels of the Cen and peak, implying unstable distributions of R and L. These mura defects of a small number of pixels are widely distributed throughout the image histogram and have a large range. Table 1 shows the ratio and range for our 200 sample images.

Table 2 Types of sample images used in detection and detection rate.

Types	Property	Number of images	Detection rate
Spot mura	Black	28	96.9% (31/1)
	White	4	
Region mura	Black	60	94.8% (128/7)
	White	75	
Impurity	Black	14	100% (14/0)
Complex mura		19	89.4% (17/2)

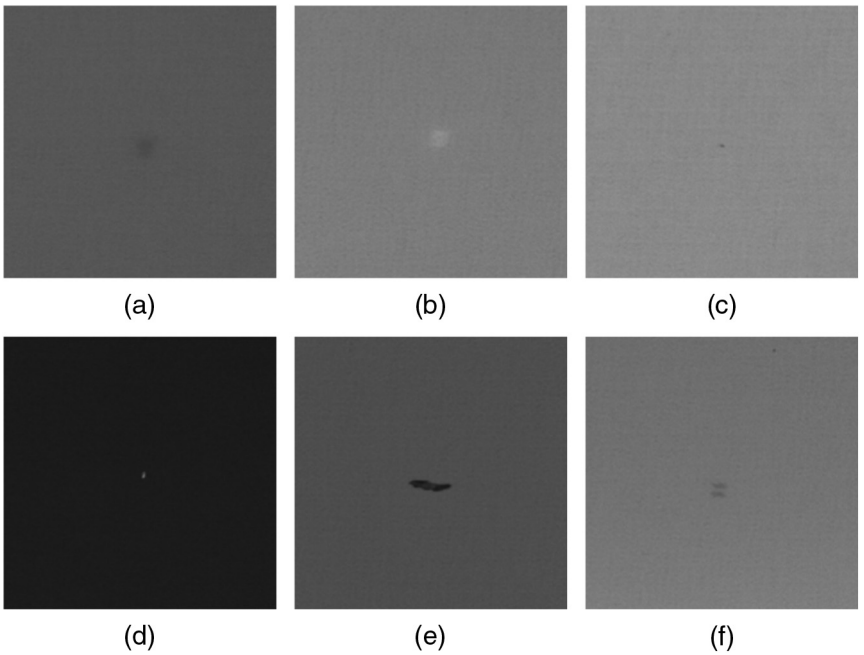

Fig. 10 Sample images used in the evaluation of reliability: (a) black region mura image of bright background, (b) white region mura image of black background, (c) black spot mura image of bright background, (d) white spot mura image of black background, (e) impurity mura image, and (f) complex mura image.

Using the above ratio and inflection point, the range of mura is defined as follows:

$$P_M = (P_G - V) : P_G, \tag{14}$$

where P_M is the range of the mura, V is the range, and P_G is the inflection point.

3.5 *Postprocessing*

When mura defects are detected by establishing the range of the mura in the images shown in Figs. 9(a) and 9(d), noise is detected in addition to mura, as illustrated in Figs. 9(b) and 9(e). To remove this noise, only mura regions are finally obtained through the median filter, as shown in Figs. 9(c) and 9(f).

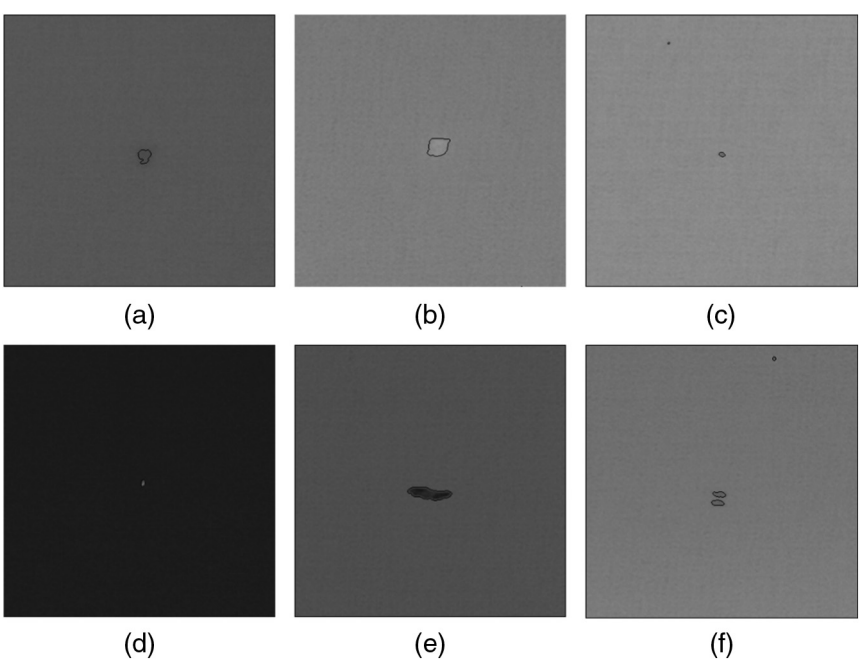

Fig. 11 Mura detection results for Fig. 10 images using the proposed method.

4 Simulation Results

4.1 *Detection Rate*

Standard images are not currently provided in the field of mura detection on display films, unlike other fields, such as face recognition, compression, and contour detection. Therefore, a large number of sample images are required since no objective comparison study on image detection rate, accuracy, and detection has been performed under the same environmental settings and conditions. Mura images on display film surface are treated as a secret by manufacturers; consequently, obtaining sample images is difficult. We obtained 200 sample images (410×410 px) from a company, which we used to evaluate our method. The results of the evaluation are displayed in Table 2. Among the total of 200 samples, mura defects were detected in 190 images and undetected in 10 images, a detection rate of 95%.

4.2 *Reliability*

This paper uses the Semu index[10] for luminance mura in FPD image quality inspection to evaluate the objective reliability of the proposed method. The Semu index[10] is defined as the ratio of $|C_x|$, the contrast between mura and background, to C_{jnd}, the minimum contrast of mura. The equation for the Semu index, $|C_x|/C_{jnd}$, is as follows:

$$\text{Semu} = \frac{|C_x|}{C_{jnd}} = \frac{\frac{|I_M - I_B|}{I_B}}{\frac{1.97}{S^{0.33}} + 0.72}, \tag{15}$$

where S^x denotes the surface area (unit: mm^2) of mura, I_M is the mean pixel value of the detected mura, I_B is the mean pixel value of the background components, C_x is the mean contrast of the detected mura (unit: %), and C_{jnd} represents the minimum contrast of the detected mura (unit: %). To evaluate the reliability, we conducted tests using sample images classified by characteristics, as shown in Fig. 10, and the mura images detected using the proposed method, as shown in Fig. 11.

Table 3 shows the mura area information and Semu when the sample images in Fig. 9 were evaluated with human vision, while Table 4 shows the sample image information and the Semu of Fig. 10 evaluated with the proposed method.

Table 3 Sample image information for Fig. 10 evaluated with human vision.

Image	Mean of background	Mean of mura	$\lvert C_x \rvert$ (%)	Size (pixel)	C_{jnd}	Semu
(a)	109.33	97.94	10.41	273	1.02	10.12
(b)	144.35	159.52	10.50	368	1.00	10.50
(c)	157.55	135.85	13.77	52	1.25	10.97
(d)	39.29	90.04	129.16	50	1.26	102.37
(e)	100.61	57.09	43.25	756	0.94	45.96
(f)	137.83	122.72	10.96	181	1.07	10.20

Table 4 Sample image information for Fig. 10 evaluated with the proposed method.

Image	Mean of background	Mean of mura	$\lvert C_x \rvert$ (%)	Size (pixel)	C_{jnd}	Semu
(a)	108.33	97.12	10.34	253	1.03	9.97
(b)	144.34	158.97	10.13	387	0.99	10.17
(c)	156.85	134.58	14.19	34	1.33	10.63
(d)	39.30	89.98	128.95	47	1.27	101.30
(e)	99.61	56.57	43.20	696	0.942	45.61
(f)	136.81	123.03	10.07	172	1.08	9.32

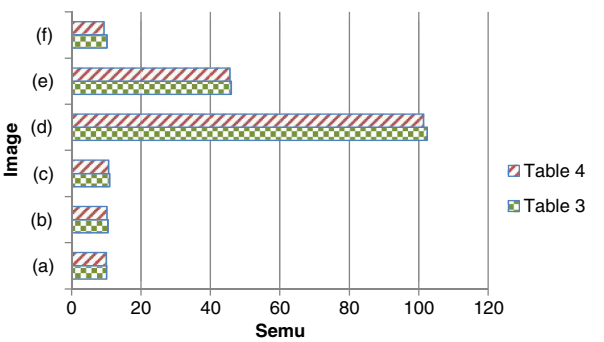

Fig. 12 Comparison of the Semu values in Table 3 (the Semu value evaluated with human vision) and Table 4 (the Semu value evaluated with the proposed method).

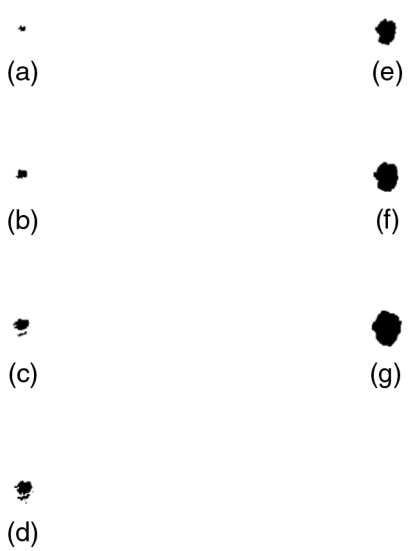

Fig. 13 Sample mura mask for Fig. 10(a): (a) −9 mask of (d), (b) −6 mask of (d), (c) −3 mask of (d), (d) original mask with mura detection, (e) +3 mask of (d), (f) +6 mask of (d), and (g) +9 mask of (d).

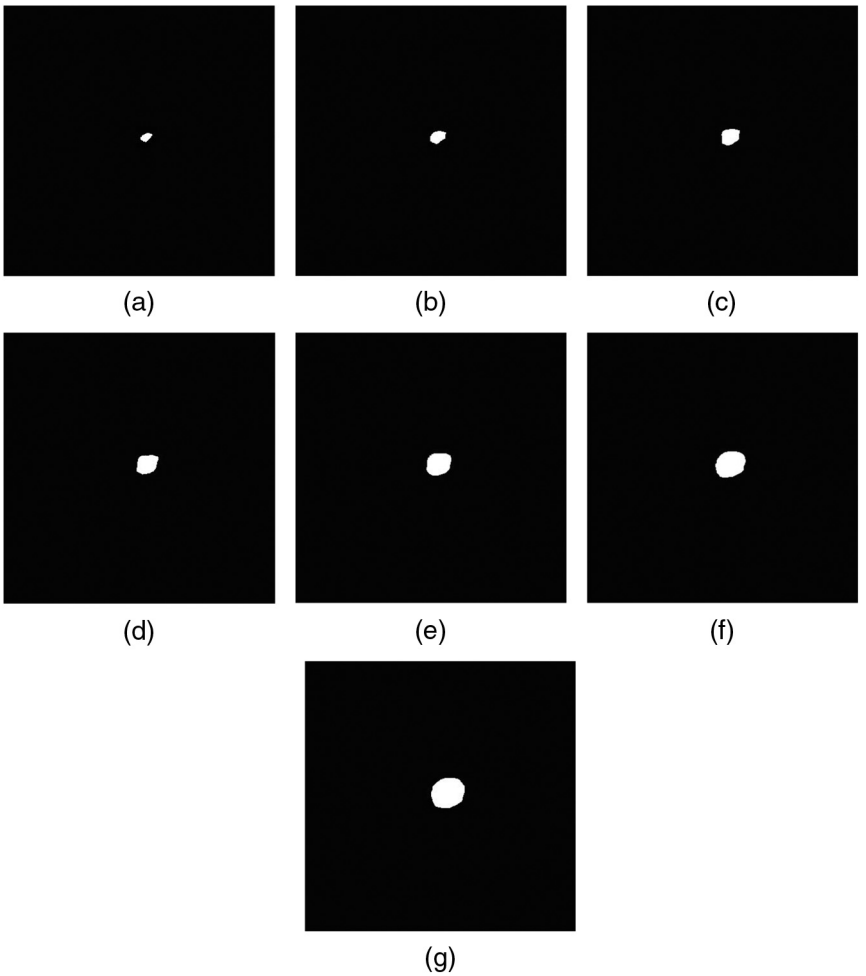

Fig. 14 Sample mura mask of Fig. 10(b): (a) −9 mask of (d), (b) −6 mask of (d), (c) −3 mask of (d), (d) original mask with mura detection, (e) +3 mask of (d), (f) +6 mask of (d), and (g) +9 mask of (d).

Figure 12 graphically compares the Semu values listed in Tables 3 and 4. It shows the successful detection rates obtained using human vision and the proposed method aligned at ~98%.

To determine how the accuracy of the Semu index varies according to mura regions detected in the images, the sample mura masks in Figs. 13 and 14 were applied to Figs. 10(a) and 10(b), respectively. Consequently, the Semu values were verified to be high as the detection area coincided with the mura area, as shown in Fig. 15.

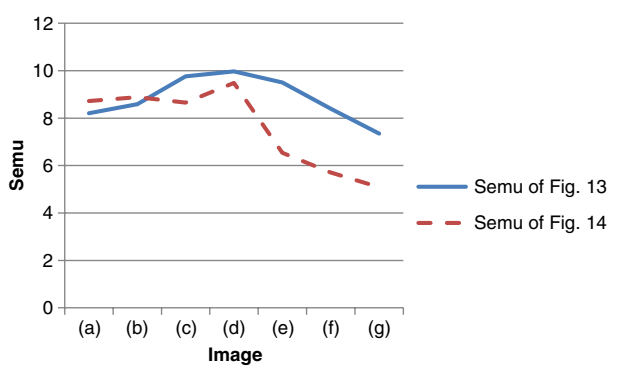

Fig. 15 Semu of Fig. 13 the value obtained by applying the Fig. 13 (sample mask of black mura) to Fig. 10(a), and Semu of Fig. 14 the value obtained by applying the Fig. 14 (sample mask of white mura) to Fig. 10(b).

Finally, we evaluated objective reliability by comparing the Semu values obtained using our proposed method with those obtained using the method proposed by Chen and Kuo.[5] For the Semu evaluation, we created images similar to those used by Chen and Kuo, as shown in Fig. 16.

Figure 17 compares the Semu values obtained by our proposed method (Table 5) with those obtained by the method developed by Chen and Kuo (Table 6). As shown in Fig. 17, the two methods give similar results for contrast6 to contrast10. However, our proposed method gives a higher Semu value for contrast1 to contrast5 and detects mura starting at contrast4. Thus, we verified that our proposed method has high reliability and accuracy.

5 Conclusion

In this paper, we proposed a method with improved ability to detect mura occurring on display film surfaces. The method uses a histogram and a constant called the Weber fraction in

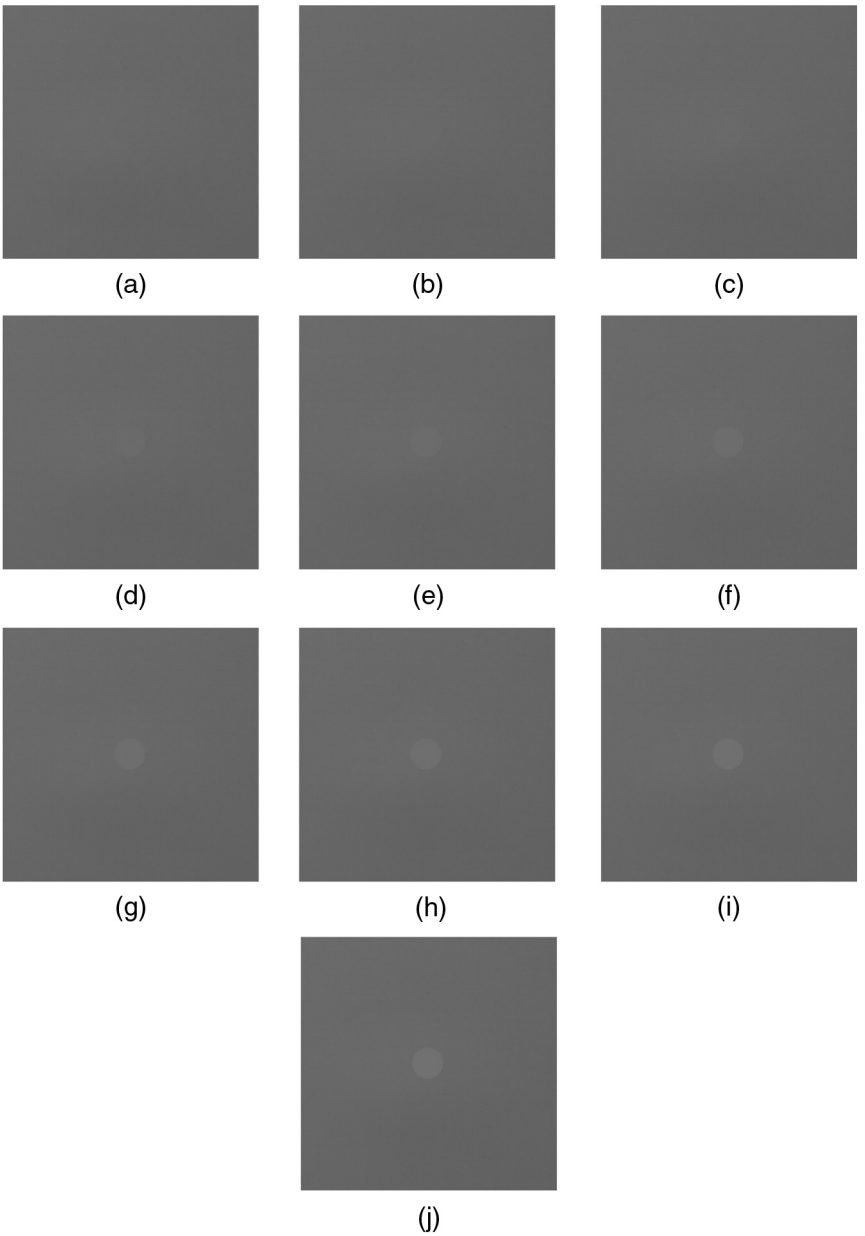

Fig. 16 Image samples used in the objective reliability evaluation: (a) contrast1, (b) contrast2, (c) contrast3, (d) contrast4, (e) contrast5, (f) contrast6, (g) contrast7, (h) contrast8, (i) contrast9, and (j) contrast10.

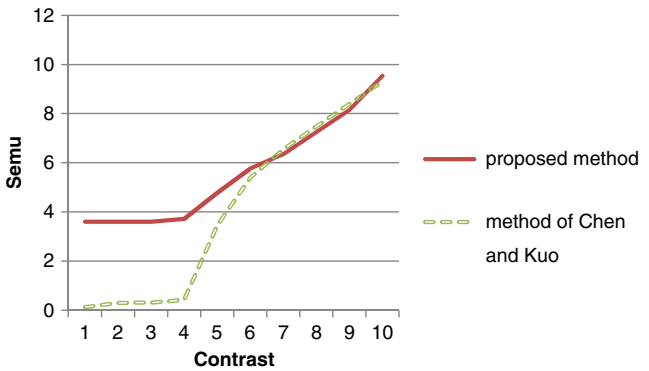

Fig. 17 Comparison of the Semu of our proposed method with that of the method proposed by Chen and Kuo.

Weber's law to detect mura. The histogram is used to discern the image information and the Weber fraction is used to select a range simulating human vision. Because it does not detect mura with a specific shape but rather the range covered by human vision, it is able to detect mura with various shapes. The results of simulations conducted using 200 varied images indicate that our proposed method has a 95% detection rate. Further, we proved that the proposed method surpassed one of the methods proposed previously as it was able to detect mura one level of contrast lower than that method. We believe that our proposed method will prove helpful in detecting various muras without being limited to a specific type of mura. However, if one image has both black and white muras, then the method will need to perform the detection procedure twice because of the

Table 5 Detection results for our proposed method.

Contrast	$\|C_x\|$ (%)	C_{jnd}	Semu	Detection
1	3.064	0.851	3.598	Failure
2	3.064	0.851	3.598	Failure
3	3.064	0.851	3.598	Failure
4	3.104	0.834	3.718	Success
5	3.976	0.834	4.766	Success
6	4.808	0.834	5.762	Success
7	5.592	0.881	6.345	Success
8	6.408	0.883	7.251	Success
9	7.208	0.883	8.155	Success
10	8.432	0.884	9.535	Success

Table 6 Detection results for the method proposed by Chen and Kuo.[5]

Contrast	$\|C_x\|$ (%)	C_{jnd}	Semu	Detection
1	0.18	1.5	0.12	Failure
2	0.37	1.28	0.29	Failure
3	0.48	1.28	0.31	Failure
4	0.52	1.22	0.43	Failure
5	3.07	0.89	3.44	Success
6	4.78	0.88	5.39	Success
7	5.79	0.88	6.55	Success
8	6.61	0.88	7.48	Success
9	7.42	0.88	8.39	Success
10	8.32	0.88	9.3	Success

characteristics of the algorithm employed, which detects mura in only one direction of the histogram. In future work, we plan to enable detection in two directions of the histogram instead of the present one direction.

References

1. V. Bruni and D. Vitulano, "A generalized model for scratch detection," *IEEE Trans. Image Process.* **13**(1), 44–50 (2004).
2. J.-S. Ryu et al., "TFT-LCD panel blob-mura inspection using the correlation of wavelet coefficients," in *Proc. 2004 IEEE Region 10 Conf.*, Vol. 1, pp. 219–222 (2004).
3. Y. Zhang, "A fuzzy neural network approach for quantitative evaluation of mura in TFT-LCD," in *Proc. Int. Conf. on Neural Networks and Brain*, pp. 424–427 (2005).
4. W.-C. Li and D.-M. Tsai, "Defect inspection in low-contrast LCD images using Hough transform-based nonstationary line detection," *IEEE Trans. Ind. Inform.* **7**(1), 136–147 (2011).
5. L.-C. Chen and C.-C. Kuo, "Automatic TFT-LCD mura defect inspection using discrete cosine transform-based background filtering and 'just noticeable difference' quantification strategies," *Meas. Sci. Technol.* **19**(1), 015507 (2008).
6. A. M. Haun and E. Peli, "Perceived contrast in complex images," *J. Vis.* **13**(13), 1–21 (2013).
7. W. S. Stiles, "Color vision: the approach through increment-threshold sensitivity," *Proc. Natl. Acad. Sci. USA* **45**(1), 100–114 (1959).
8. F. L. Van Nes and M. A. Bouman, "Spatial modulation transfer in the human eye," *JOSA* **57**(3), 401–406 (1967).
9. P. Whittle, "Increments and decrements: luminance discrimination," *Vis. Res.* **26**(10), 1677–1691 (1986).
10. SEMI., "Definition of measurement index (SEMU) for luminance mura in FPD image quality inspection," SEMI D31-1102, Semiconductor Equipment and Materials International (2006).
11. F.-M. Tzu and J.-H. Chou, "Spot mura evaluation in TFT-LCDs using automatic optical inspection," in *Proc. 5th IEEE Int. Conf. on Microsystems Packaging Assembly and Circuits Technology*, pp. 1–4 (2010).
12. Y.-C. Lee, C.-E. Shie, and D.-C. Tseng, "LCD mura detection based on accumulated differences and multi-resolution background subtraction," in *Proc. 5th Fifth Int. Conf. on Image and Graphics*, pp. 189–194 (2009).
13. H. C. Shao et al., "Robust segmentation for automatic detection of mura patterns," in *13th IEEE Int. Symp. on Consumer Electronics*, pp. 267–270 (2009).
14. C. Zhuang and H. Ding, "A new mura defect inspection way for TFT-LCD using level set method," *IEEE Signal Process. Lett.* **16**(4), 311–314 (2009).
15. W.-H. Kao, J. C. Hung, and V. Hsu, "Using data mining techniques in development of mura geometric prediction module for large area photomask," in *Proc. IEEE Asia-Pacific Services Computing Conf.*, pp. 957–962 (2008).
16. W. Li, W. Yang, and Q. Liao, "Illumination normalization based on Weber's law with application to face recognition," *IEEE Signal Process. Lett.* **18**(8), 462–465 (2011).

Myung-Muk Kim is a researcher at the Korea Aerospace Research Institute. He received his BS and MS degrees in electronic engineering from Hanbat National University in 2012 and 2014, respectively. His current research interests include image processing, layout design, and android porting.

Seung-Ho Lee is a professor at Hanbat National University. He received his BS and MS degrees in electronic engineering from Hanyang University in 1986 and 1989, respectively, and his PhD degree in electronics from Hanyang University in 1994. He is the author of more than 30 journal papers and has written 17 book chapters. His current research interests include image processing, embedded system, and VLSI&CAD.